Check for updates

Enhancing corrosion resistance of mild steel in hydrochloric acid with *Chiquita* banana sap extract†

Nhon Pham Van,‡[ab] Ngoc Cam Tu Hoang, [iD] ‡[ab] Tran Dinh Manh,[c] Le Thuy Dung,[d] Nguyen Si Hoai Vu,[ab] S. V. Prabhakar Vattikuti,[e] Casen Panaitescu, [iD] [f] Trung T. Pham[g] and Nam Nguyen Dang [iD] *[ab]

The corrosion of metals is still a huge challenge for various industries, and the pursuit of effective treatments ensures environmental sustainability. In this study, we utilized *Chiquita* banana sap–water extract (BSWE) to prevent mild steel from electrochemical corrosion in a 0.1 M HCl at room temperature. Corrosion resistance was assessed using various electrochemical methodologies, combining with surface characterization techniques. The results showed a high level of effectiveness when the corrosion current density decreased from 3292.67 $\mu A\ cm^{-2}$ (for the sample immerged in the blank solution) to 187.33 $\mu A\ cm^{-2}$ after 24 hours of immersion in the solution containing BSWE at a 2000 ppm concentration, equivalent to corrosion efficiency of 94.32%. Surface characterization revealed diminished corrosion on the inhibited steel surface due to the formation of a protective layer. X-ray photoelectron spectroscopy results demonstrated the presence of BSWE ingredients combining with iron oxides and hydroxides to form a smooth protective layer. Furthermore, theoretical calculations also indicated that the addition of BSWE can reduce steel surface damage when exposing to corrosive environment. The inhibitor based on banana sap extract can be referred to as a sustainable protective coating since it is biodegradable, abundantly available in banana plants and free of other harmful substances.

1. Introduction

The phenomenon of acid corrosion in mild steel has increasingly attracted attention due to its severe impact on various industrial sectors, resulting in substantial annual financial implications running into billions of dollars. Corrosion not only diminishes the durability of materials but also triggers significant expenses due to frequent replacements and productivity

drops.[1,2] The urgency to address this issue is amplified by the significant implication on various industrial sectors.[3] Consequently, it is imperative to forecast the structural performance of metal constructs and offer solutions to mitigate the challenges posed by corrosion.[4] In this context, the employment of inhibitors emerges as an indispensable and widely adopted strategy to prevent the corrosion-induced dissolution of mild steel and other metals.[5–7] Although many synthetic compounds have proven effectiveness in providing anti-corrosion properties, a major drawback is their negative impact on human health and the environment.[8,9] The global concern regarding safety and sustainability issues associated with corrosion inhibitors in various industries has been a persistent issue.[10] However, the widespread application of these inhibitors is hindered by the long-term toxicity effects, related to the synthesis stage and practical applications.

In recent years, there are a development of eco-friendly corrosion inhibitors, such as natural products like plant extracts and animal proteins,[11–14] rare earth elements,[15] and organic compounds.[16,17] Plant-based products are particularly favored due to their low-cost, availability, and renewable sources, making them a green option for inhibitors.[18–20] These inhibitors work by the formation of a protective layer through the deposition of reaction products, thereby preventing further corrosion of metallic substrates.[21] Numerous studies have

aFaculty of Civil Engineering, Duy Tan University, Danang 550000, Vietnam. E-mail: nguyendangnam@duytan.edu.vn

bFuture Materials & Devices Lab., Institute of Fundamental and Applied Sciences, Duy Tan University, Ho Chi Minh City 700000, Vietnam

cInstitute of Applied Technology, Thu Dau Mot University, 6 Tran Van on Street, Phu Hoa Ward, Thu Dau Mot City, Binh Duong 820000, Vietnam

dPetrovietnam Manpower Training College, 762 Cach Mang Thang Tam Street, Long Toan Ward, Ba Ria City 790000, Vietnam

eSchool of Mechanical Engineering, Yeungnam University, Gyeongsan 38541, Republic of Korea

fDepartment of Petroleum Geology and Reservoir Engineering, Petroleum-Gas University of Ploiesti, 100680 Ploiesti, Romania

gNamur Institute of Structured Matter (NISM), Department of Physics, University of Namur, 61 Rue de Bruxelles, Namur B-5000, Belgium

focused on plant extracts as a mean of preventing steel corrosion.[18,19,22,23] Plant extracts contain a wide range of polar and non-polar organic compounds that can create reactions with metal surfaces to prevent corrosion with minimal effect on the environment.[23] Particularly, organic compounds comprise functional groups (OH, COOH, C=O, *etc.*) and heteroatoms like oxygen (O), nitrogen (N), sulfur (S), and phosphorus (P), which significantly influence the protective performance of the corrosion inhibitor. Moreover, the strength of the covalent bond between these heteroatoms can be used to predict the potential efficacy of the inhibitor.[24] For banana pulp, it contains polyphenols (phenolic acids and flavonoids), and vitamins,[25,26] presenting a promising avenue for sustainable utilization of agricultural waste in corrosion prevention. Although these compounds have been used frequently in corrosion mitigation, they are limited due to their complex organic compositions. Factors such as plant species, location, season, and environmental conditions, which can greatly influence the composition and concentration of organic compounds, leading to inconsistent performance in prevent metal from corrosion.[27] Moreover, the slow decomposition of banana leaves can result in the formation of deposits that may clog pipes and damage machinery. Banana sap could replace to banana leaves due to its availability and potential for eco-friendly materials. Banana trees, belonging to the monocotyledon annual herbaceous plant group (family Musaceae),[28] are cultivated in over 130 countries and are among the most widely consumed fruits globally after citrus fruits.[29] After harvesting, these banana trees cannot be used for the next harvest, leaving behind substantial biomass containing valuable organic components.[30] The abundance of agricultural waste can be used to convert these readily available resources into products with a higher value, especially banana sap. Besides, tannins present in banana sap cause the sap to darken when exposed to air, demonstrating appearance of carbohydrate and suggesting its potential for long-term rust prevention with environmentally sustainable properties.[31,32]

The main objective of this investigation is to study the electrochemical response of natural plant waste to mitigate the corrosive effects of hydrochloric acid on mild steel. To achieve this, we used a banana sap-water extract (BSWE) to limit the deterioration of mild steel, which is known to be prone to corrosion in acidic environments. Additionally, the study aims to analyze different adsorption models to understand inhibitory mechanism of BSWE. The primary focus is to assess the impact of inherent characteristics of BSWE in the hydrochloric acid medium at an optimal concentration. This gives insight in its ability to enhance the corrosion resistance of mild steel through a combination of experimental methods and simulation. This study not only enhances comprehension of electrochemical behaviors of steel in an acidic medium but also shows potential anti-corrosive application of banana sap for developing an effective corrosion inhibition.

2. Experimental section

All chemicals were utilized to synthesize *Chiquita* banana sap-water extract and prepare the 0.1 M HCl solution (pH = 1)

that was purchased from Merck KgaA and employed exactly as provided. Other chemicals included distilled water, 37% HCl, ethanol, and methanol. The sap was harvested from the peduncle of unripe fruits of *Chiquita* banana from South Vietnam, specifically the position near the stem where sap concentration is the highest. The collected sap was combined with the investigated solution and a filter was used to determine the employed concentration. Gas chromatography-mass spectrometry (GC-MS) was employed to characterize the primary component of BSWE at a flow rate of 1 mL min^{-1}. BSWE was dissolved in the HCl solution with varying concentrations of 500, 1000, 1500 and 2000 ppm.

Mild steels were immersed in a 0.1 M HCl solution without and with varying concentrations of BSWE at room temperature (25 °C). The corrosion behavior of steels was investigated using electrochemical impedance spectroscopy (EIS), potentiodynamic (PD) and potentiostatic (PS) polarization, and linear polarization resistance (LPR) measurements. Three-electrode system was employed, including an Ag/AgCl/KCl$_{sat}$ electrode as the reference electrode (R.E.), a titanium mesh as the counter electrode (C.E.), and an AS1020 mild steel rod as the working electrode (W.E.) with composition in Table S1.† The AS1020 was encased in epoxy resin to ensure the flat surface with 1 cm^2 of exposed area. Prior to experimentation, the working surfaces were ground with various types of silicon carbide papers (100, 400, 800, 1000, and 1200 grits), followed by cleaning in an ultrasonic ethanol bath, washing, and drying with a hair dryer. All measurements were conducted using a VSP Potentiostat connected to a computer running the commercial EC Lab program. To establish a stable state of the open circuit potential (OCP), the working electrode was immersed in the prepared solution for 1 hour before each experiment. Potentiodynamic polarization measurements involved automatically varying the electrode potential from −250 mV *vs.* OCP to 0 mV relative to $V_{Ag/AgCl}$ at a scan rate of 0.166 mV s^{-1} at 25 °C. Additionally, changes in anodic current density of −450 mV$_{Ag/AgCl}$ as a function of immersion time for steel after 24 hours of immersion in the solution, which were characterized by a potentiostatic test. For electrochemical impedance spectroscopy (EIS) studies, the cell was subjected to a modest alternating voltage disturbance (10 mV) over the frequency range of $10^4 \div 10^{-2}$ Hz. Finally, linear polarization resistance (LPR) measurements were undertaken every 1 hour for 24 hours at OCP with a scan rate of 0.166 mV s^{-1} over a potential range of ±20 mV$_{OCP}$. Each condition was performed three times to ensure the repeatability and accuracy of the results.

After 24 hours of immersion at OCP, the morphological properties of the steel surface were determined using field emission scanning electron microscopes (FE-SEM, Hitachi S-4800). Furthermore, steel surfaces after corrosion were also evaluated using X-ray photoelectron spectroscopy (XPS).

Simultaneously, after the analysis of the GC-MS method and the results suggested in Fig. S3 and Table S2.† Three substances were identified from the *Chiquita* banana sap extraction that had the highest matching probabilities from the results and database, including capsaicin (C$_{18}$H$_{27}$NO$_3$ – MC1), dihydrocapsaicin (C$_{18}$H$_{29}$NO$_3$ – MC2), and spirohexan-5-one (C$_6$H$_8$O

– MC3). These substances were representative of BSWE for all following simulations. The BSWE molecular structures were grabbed from PubChem open database and subsequently introduced to the Materials Studio program (MS) for quantum chemical (DFT) and molecular dynamics (MD) calculations. The DFT and MD simulations were performed by the DMol³ and Forcite modules of the MS, which employed the following settings. For DFT calculation, all three MC substances (MC1, MC2, and MC3) suffered structural optimization and energy calculation with B3LYP hybrid functional, Gimme's diffusion correction function (D), and double numerical atomic polarization (DNP) basis sets were applied. The considered quantum chemical parameters included the frontier molecular orbitals (FMO) and the Fukui electrophilic f(−) and nucleophilic f(+) indices. The FMO comprises the highest occupied (HO) and the lowest unoccupied (LU) molecular orbitals (MO). There is a close relationship between the construction of HOMO/LUMO regions and Fukui f(−)/f(+) indices. The HOMO region is already filled with electrons, giving electrons to positively charged species (electron-deficient species or nucleophiles) and undergoing nucleophilic attack. This region (HOMO) corresponds to the Fukui f(−) index defined by FMO theory. The same argument applies to the LUMO region, which is nearly electron-empty and thus tends to gain electrons from negatively charged species (electron-rich species or electrophiles) and undergo electrophilic attack. This region (LUMO) corresponds to the Fukui f(+) index defined by FMO theory.

For MD calculation, an optimized structure of MC1, MC2, or MC3 (obtained from DFT simulation) was put in a simulation box with a Fe(110) substrate, 556 water molecules, one oxonium ion, and one chloride ion to mimic the corrosive environment (0.1 M HCl). The dimensions of the simulation boxes and the steel substrate were adjusted to match the size of each MC molecule. MD simulation was performed at 298 and 333 K (25 and 40 °C), employed canonical ensemble (NVT) and COMPASS force field. The MD simulation was conducted in a 1.0 ns trajectory, with a 1.0 fs time step (10^6 steps). The temperature of the box was maintained at a stable level throughout the simulation using a heat bath and the Andersen thermostat algorithm for every 1.0 ps.

To quantitatively evaluate the interaction between the adsorbent molecule and the surface, binding energy (E_b) and binding energy per atom (E_b per atom) for each MC molecule were conducted eqn (1)–(4). Comparing E_b between molecules with different atom numbers may lead to misinterpretation because MD simulations are performed on an atomic scale (interested in particle–particle rather than object–object interactions).[33,34] The authors propose to evaluate the adsorbent/adsorbate interaction *via* E_b per atom (eqn (2)–(4)), which is calculated by dividing E_b (of eqn (1)) by the total number of particles of each MC substance to assist E_b in a more objective assessment of the interaction.

$$E_b = -[E_{all} - (E_{sub+sol} + E_{inh+sol}) + E_{sol}] \quad (1)$$

$$E_b \text{ per atom} = |E_b|/49, \text{ for MC1} \quad (2)$$

$$E_b \text{ per atom} = |E_b|/51, \text{ for MC2} \quad (3)$$

$$E_b \text{ per atom} = |E_b|/15, \text{ for MC3} \quad (4)$$

E_{all}, $E_{sub+sol}$, $E_{inh+sol}$, and E_{sol} in eqn (1) are the boxes' total energy comprising all species, substrate and solution, inhibitor and solution, and the standalone solution at the last MD stages (after 1.0 ns of trajectories).

3. Results and discussion

Fig. 1(a) illustrates electrochemical behaviors of the steel surface through potentiodynamic polarization curves. This analysis is based on a plot of current density against potential, facilitating the determination of various electrochemical parameters. As observed in the figure, mild steel exposed to the blank HCl solution exhibits a high corrosion rate, with no evidence of the development of a protective film due to the rapid rise in current density and potentials were increased in the anodic branch. In the fact that the nature of steel is an active material, therefore, it is easy to create redox reactions in an electrochemical system. Notably, the current density of steel in the blank solution exhibited the highest value compared to other cases, indicating that the total electron flow generated by the redox process occurring on the steel surface was highest when no inhibitor was added to solution. It could result in a high rate of steel dissolution, leading to the highest corrosion current density performed on the uninhibited steel specimen as shown in Table 1. Upon immersion of the steel sample in BSWE-containing solutions, a significant decrease in current density was observed, accompanied by a lightly electropositive shift of the corrosion potentials. This shift is most pronounced at a concentration of 2000 ppm, where the corrosion potential increased from −560.33 to −539.67 mV$_{Ag/AgCl}$. In addition, the potentiodynamic curves exhibit notable changes in the results of inhibited specimens, particularly in the anodic branches, which exhibited a film formation due to the significant decrease in current densities when potentials increased from E_{corr} to −300 mV$_{Ag/AgCl}$. These changes could reduce the oxidizing power on the inhibited steel surfaces, leading to a significant decrease in the corrosion current density from 3292.67 to 187.33 μA cm^{-2} as shown in Table 1. Therefore, the lightly electropositive shift of the corrosion potentials and the significant decrease in corrosion current densities indicates that BSWE could act as a mixed type of inhibitor with a dominant anodic inhibition for the mild steel in 0.1 M HCl solution. The collective results strongly suggest the inhibitory effectiveness of BSWE, as depicted in Table 1 and Fig. 1(b). The inhibition efficiency increased from 48.76 to 94.32% as the concentration of BSWE ranged from 500 to 2000 ppm.

Furthermore, the trend of the OCP of steel samples when exposed to acid media with 0 and 2000 ppm BSWE addition, as illustrated in Fig. 1(c). The OCP of steel specimens was gradually decreased over time in both cases, but the decrease in OCP values was more obvious observation on the uninhibited specimen. However, when 2000 ppm BSWE was added to the investigated solution, OCP of steel exhibited more
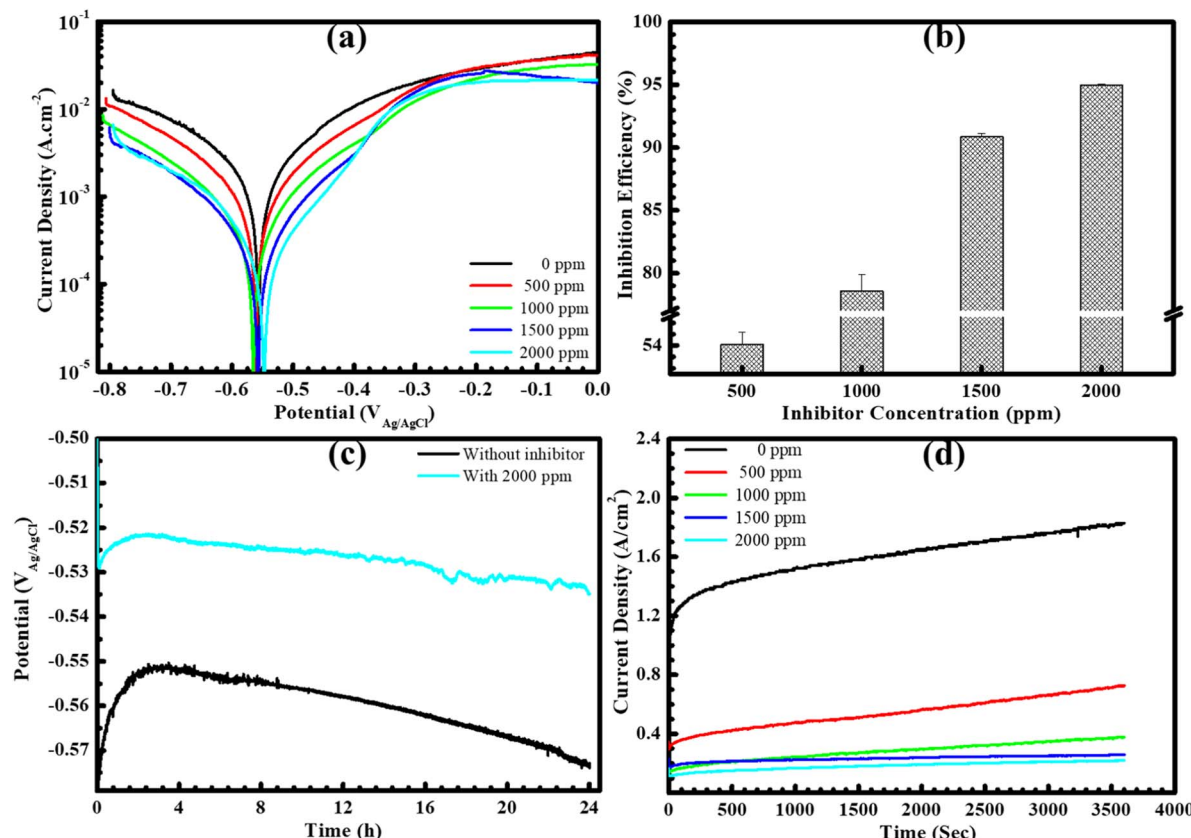
Fig. 1 (a) Represented potentiodynamic polarization, (b) effect of BSWE concentration on inhibition efficiency, (c) open circuit potential, and (d) change of anodic current density at -450 mV$_{Ag/AgCl}$ as function of immersion time for steel after 24 h immersion in solution.

electropositive values and stability during 24 h of the immersion time. Importantly, the shift of OCP agreed with that of corrosion potential, observed on the PD results. Therefore, the electropositive OCP and corrosion potentials of steel in a 0.1 M HCl could be due to the BSWE addition. To corroborate the results of the PD analysis, a potentiostatic polarization test was conducted at a constant anode potential of -450 mV$_{Ag/AgCl}$ (Fig. 1(d)). This potential was assessed in the stability of the protective layer through the PD analysis. The results shown in Fig. 1(d) demonstrate a significant decrease in anodic current density as the concentration of BSWE in corrosive solution, compared to the uninhibited sample (1.2–1.8 A cm^{-2}). The decrease in current density can be explained by the formation of a robust and firmly attached protective layer. This protective film effectively hinders electrochemical reactions occurring at anode sites, hence inhibiting corrosion. Importantly, PD results

consistently show changes in current density, demonstrating the effectiveness of BSWE in inhibiting corrosion and the high repeatability of the polarization methods. Corrosion kinetic parameters including the corrosion potential (E_{corr}) and current density (i_{corr}) are summarized in Table 1 to evaluate the corrosion resistance of the samples. The following equation offers the value of the inhibitory effect:

$$\eta = \frac{i_{corr}^{o} - i_{corr}}{i_{corr}^{o}} \times 100\% \tag{5}$$

where η represents the inhibitory efficiency, i_{corr} and i_{corr}^{o} denote the corrosion current densities with and without the inhibitor, respectively. These current density values are calculated using the Tafel extrapolation method. Comparative inhibitor performance demonstrates that the increasing addition of BSWE leads to a significant increase in inhibition efficiency. As

Table 1 Corrosion parameters obtained from potentiodynamic polarization curves

Specimens	E_{corr} (mV$_{Ag/AgCl}$)	i_{corr} (μA cm^{-2})	β_a (mV per decade)	$-\beta_c$ (mV per decade)	η (%)
0 ppm	$-560.33 \div 1.83$	$3292.67 \div 513.67$	$282.67 \div 28.67$	$340.33 \div 48.83$	
500 ppm	$-557.00 \div 4.00$	$1587.67 \div 123.33$	$249.67 \div 18.33$	$262.33 \div 21.67$	$48.76 \div 4.12$
1000 ppm	$-557.33 \div 4.67$	$800.00 \div 38.50$	$208.67 \div 14.83$	$216.33 \div 25.17$	$75.78 \div 1.51$
1500 ppm	$-553.67 \div 4.83$	$341.00 \div 7.50$	$163.33 \div 4.67$	$190.00 \div 15.00$	$89.66 \div 0.29$
2000 ppm	$-539.67 \div 4.17$	$187.33 \div 2.67$	$132.00 \div 5.00$	$154.33 \div 20.67$	$94.32 \div 0.10$

indicated in Table 1, mild steel immersed in a solution containing BSWE at a concentration of 2000 ppm exhibits better corrosion resistance compared to other concentrations. Specifically, the lowest i_{corr} and the highest corrosion inhibition efficiency (94.32%) demonstrated the outstanding protection provided by this inhibitor.

The linear relationship between voltage and current for all steel samples was successfully established through the analysis of linear polarization resistance, as illustrated in Fig. 2(a). Notably, the current density showed a significant decrease as the increased of BSWE concentration from 0 to 2000 ppm BSWE. For a more detailed insight into this outcome, Fig. 2(b) presents the alterations in polarization resistance (R_p), indicating an increase in values with rising BSWE concentrations spanning from 0 to 2000 ppm and across different immersion times. Specifically, at a concentration of 2000 ppm, the polarization resistance exhibited a rapid increase within the initial 7 hours, followed by a stabilization of the R_p value in subsequent hours. These LPR findings align with the PD results, confirming that BSWE effectively inhibits steel corrosion in the investigated solution.

To evaluate the corrosion mechanism of steel under varying concentrations of BSWE in the corrosive solution, the electrochemical impedance spectroscopy data for each case is presented in Fig. 3. In the case of a blank solution, as depicted in Fig. 3(a), the initial impedance value was high in the first hour, but then decreased in subsequent hours before increasing again towards the end of the immersion time, corresponding to corrosion of the steel. Subsequently, as corrosion products established on the steel surface, the corrosion rate decreased and there was a slight increase in the impedance value. In the cases when BSWE was added, the total impedance value increased significantly, particularly at a concentration of 1500 ppm. The increase in the display arc diameter size demonstrated the formation of a protective layer on the steel surface after 24 hours of immersion. At a concentration of 2000 ppm, the impedance value is significantly high, but there is no linear increase, from 1 to 12 h. Moreover, the impedance value continues to increase and stabilize in the following hours. The Nyquist plots for

various BSWE concentrations within the investigated frequency range show a dual-time constant behavior. This indicates that the interface between the samples and the electrolyte can be accurately described by the parallel arrangement of transfer resistance charge (R_{ct}) and constant phase element (CPE). These elements are connected in series with film resistance and run in parallel with another CPE. Fig. 3(f) illustrates the simulated equivalent circuit, which includes the phase elements associated with the protective layer (CPE_1) and the charge transfer layer (CPE_2). This proposed circuit captures the intricacies of the system, providing a comprehensive representation of the electrochemical behavior observed in the Nyquist plot.[35] To analyze the parameters obtained from EIS, the ZSimpWin software was used to create an equivalent circuit using experimental data. The compatibility of the equivalent circuit was determined by the least difference between the experimental and analytical results, with a Chi square (χ^2) value of less than 10^{-3}. The impedance results, shown in Fig. 3(a–e), demonstrate a high level of agreement between the analyzed spectrum and the experimental results. Futhermore, Bode plots are presented in Fig. S1 and S2.† Throughout the cascade form, there is a noticeable increase in the impedance magnitudes |Z| (Fig. S1†) as the concentration of BSWE increases, indicating an improvement in protective performance. This is further supported by the critical values of the phase angle (θ) depicted in the Bode phase plot (Fig. S2†), which demonstrate a greater inhibitory behavior is achieved when increasing BSWE concentration in an acidic solution (Fig. S2†). The analytical data shown in Fig. 4 displays a gradual decrease in the CPE_{dl} (CPE of double layer) and CPE_{pro} (CPE of protective layer) values of steel electrodes when exposed to solutions containing BSWE at various concentrations (0–2000 ppm) for 24 hours. In the case of a blank solution and a concentration of 500 ppm BSWE, CPE_{pro} values tend to increase over time. However, low CPE_{pro} values are observed in higher BSWE concentrations due to limit ion penetration into the steel surface. Additionally, the mild steel exposed to blank solution exhibited very low R_{pl} and R_{ct} values in Fig. 4(c and d). The obtained results indicated strong electron transfer and fast electrochemical corrosion reactions.
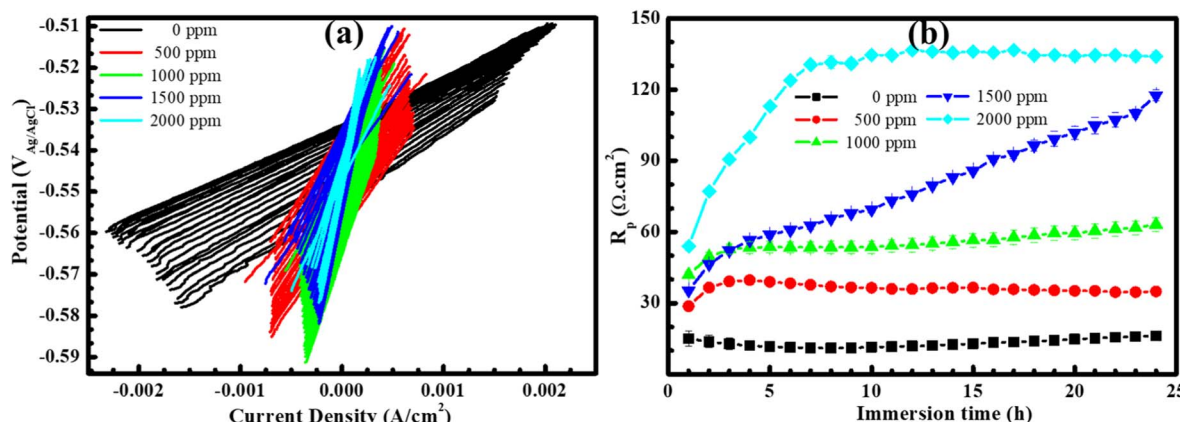

Fig. 2 (a) Linear polarization resistance (LPR) measurements and (b) the polarization resistance derived from the steel's LPR data following a 24 hours immersion in solution.
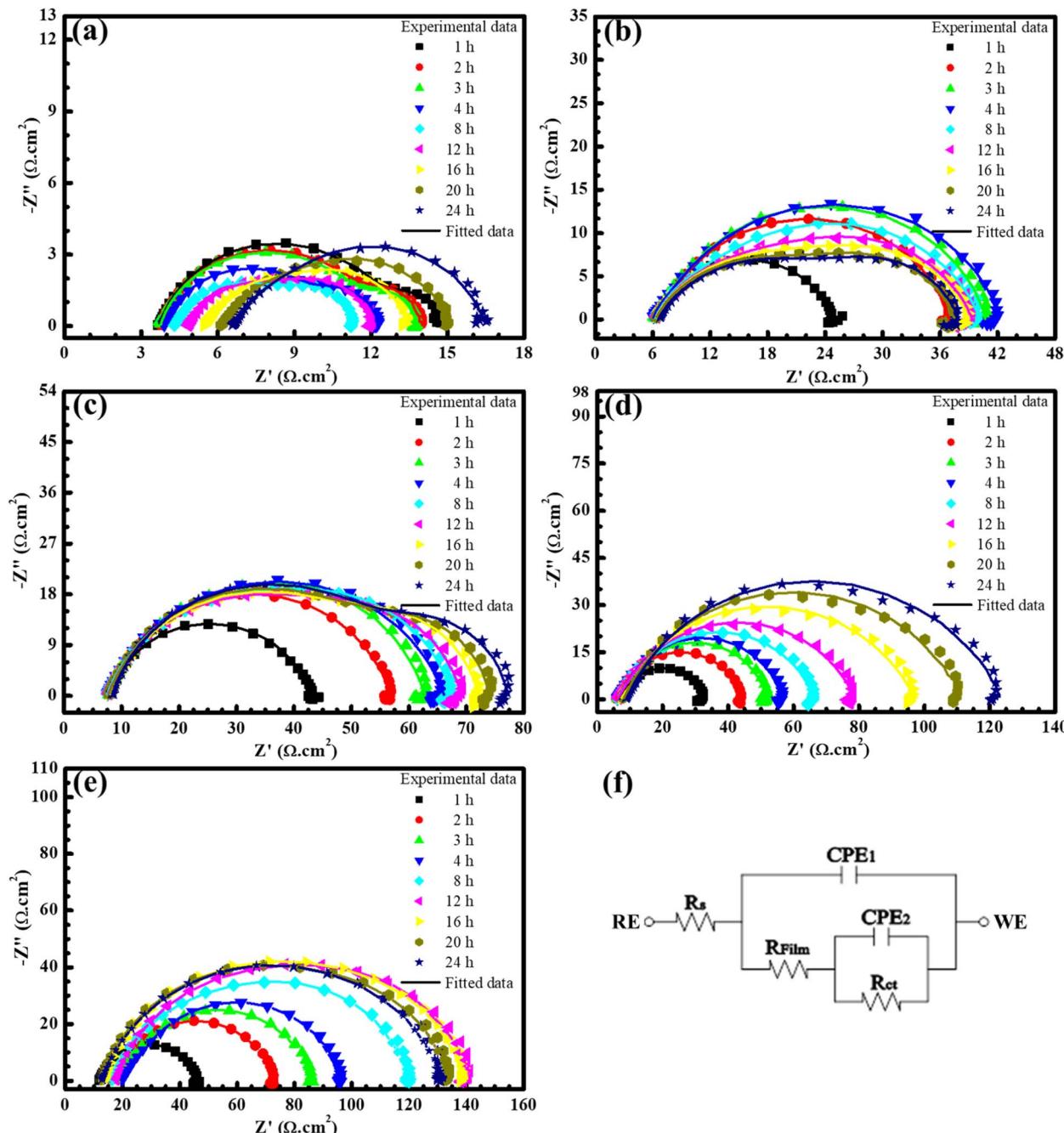
Fig. 3 Electrochemical impedance spectroscopy (EIS) results of steel in (a) 0, (b) 500, (c) 1000, (d) 1500, and (e) 2000 ppm, and (f) equivalent circuit for fitting EIS data.

As the BSWE concentration approaches 2000 ppm, the EIS values demonstrate the formation of a protective film on the entire electrode surface, resulting in high corrosion resistance.

The SEM images in Fig. 5 illustrate significant changes in the morphology of steel surfaces before and after being immersed in solutions with varying concentrations of BSWE for 24 hours, compared to the raw grinding steel surface. They clearly show the effective influence of BSWE on the steel surfaces. In Fig. 5(a), the abrasive steel surface still exhibits residual grinding marks at a detailed level. Nevertheless, when exposure

to a corrosive solution without the inhibitor, Cl⁻ ions cause significant degradation of the steel surface, as evidenced in Fig. 5(b). This is due to a combination of external and internal factors that make certain areas of the steel surface more susceptible to corrosion. These areas often have imperfections and weaknesses in the protective oxide layer, making them more prone to corrosion. Additionally, defects within the material's structure can also contribute to localized corrosion, such as pitting corrosion.[36] Conversely, when the inhibitor BSWE is added at varying concentrations, substantial changes
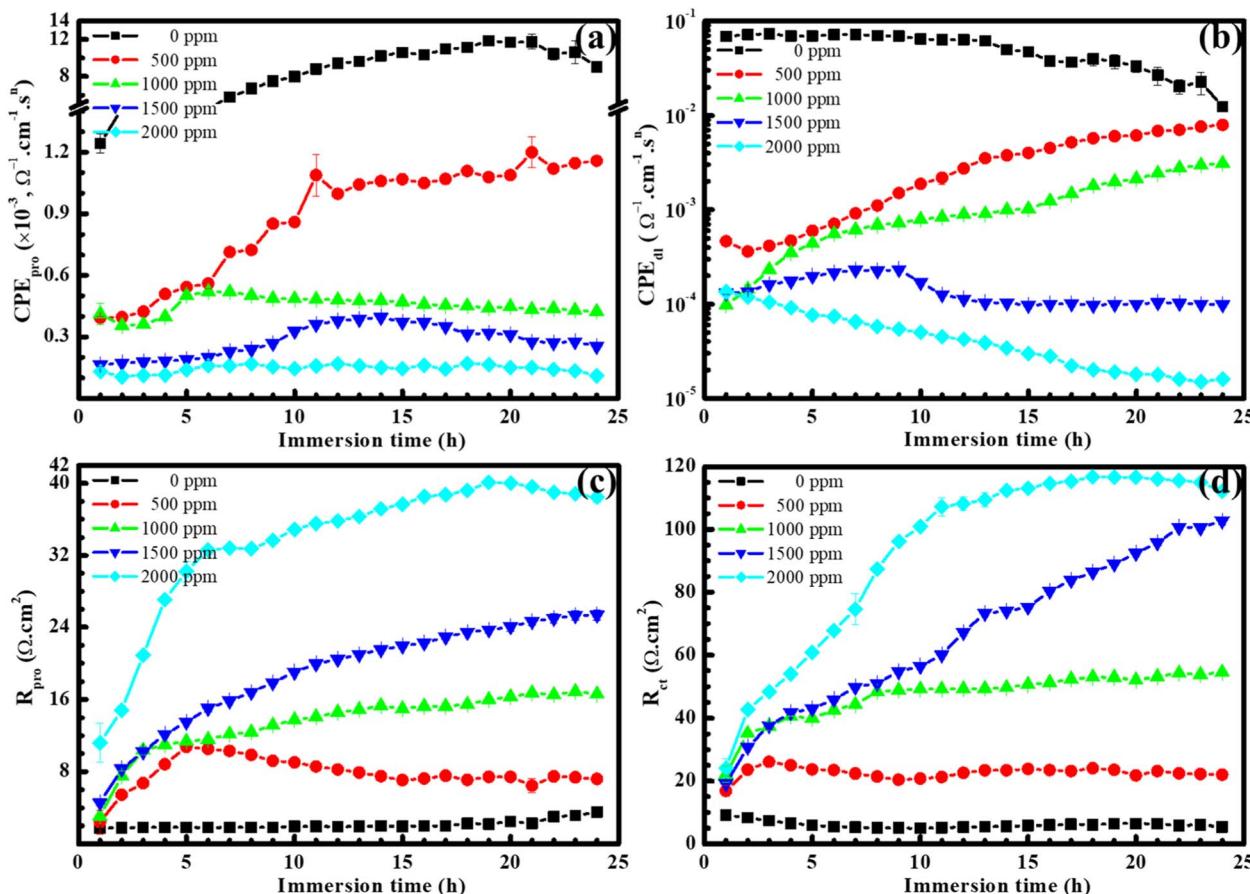
Fig. 4 Effect of BSWE concentration on CPE magnitudes of (a) protective layer and (b) double layer, (c) protective layer and (d) charge transfer resistances.

in morphology of steel surface can be observed. At a concentration of 500 ppm BSWE, a thin film begins forming on the surface, as depicted in Fig. 5(c). The film is believed to be the result of the grinding marks becoming less visible after exposure to the investigated solution. This formation of protective film becomes even more noticeable at concentrations of 1500 ppm and particularly at 2000 ppm BSWE, as seen in Fig. 5(e and f). In these images, the steel surface displays a more distinct layer of the thin film, both clustered and scattered across the steel surface. Notably, the structure of the protective layer plays a pivotal role in regulating the corrosion rate of mild steel as immersed in the corrosion solution. At a BSWE concentration of 2000 ppm, the mild steel surface displays a more uniformly distributed and agglomerated protective layer. As a result, it offers an enhanced hindrance to the inward diffusion of corrosive species into the underlying substrate. This structural benefit is crucial in controlling corrosion. The components of the protective layer, as demonstrated later in XPS analyses, contribute significantly to its overall effectiveness.

Corrosion products and the film formation on the steel surface necessitate thorough investigation and evaluation, as they are vital to explain the mechanism of corrosion inhibitor BSWE. As previously hypothesized, it is believed that the protective layer is formed through the adsorption of organic

groups from BSWE and ions present in the raw steel composition. To confirm this, XPS analysis was performed on steel samples immersed in the investigated acid solution for 24 hours, both with and without the addition of 2000 ppm BSWE. The obtained results revealed the presence of certain elements, including Fe, C, and O in the wide scanning region (Fig. 6(a)).[37,38] The positions of the satellite peaks for these signals were highly sensitive to oxidation states, allowing for a qualitative determination of the ionic states of iron. In Fig. 6(b) and (c), the peak intensity of Fe indicates a significant amount of organic matter participating in Fe bonding. In the absence of the inhibitor, the Fe 2p peaks appeared broader with lower binding energies ranging between 710 and 725 eV ($E_b = $ 720 eV). The appearance of Fe $2p_{3/2}$ spectra at 710 eV suggests the presence of iron salts and oxide products such as Fe_2O_3, Fe_3O_4, and FeOOH.[39] Similarly, the presence of the Fe $2p_{1/2}$ spectrum in the spectral range of 720–725 eV indicated the existence of iron oxides and metallic iron.[40] The strong intensity of the Fe 2p structure presents that these products primarily existed in the absence of inhibitors, specifically iron products when subjected to an environment rich in Cl^- ions. Interestingly, when the BSWE inhibitor was added at a concentration of 2000 ppm, as shown in Fig. 6(b), the intensity of the Fe 2p structure decreased, with the disappearance of a specific peak at
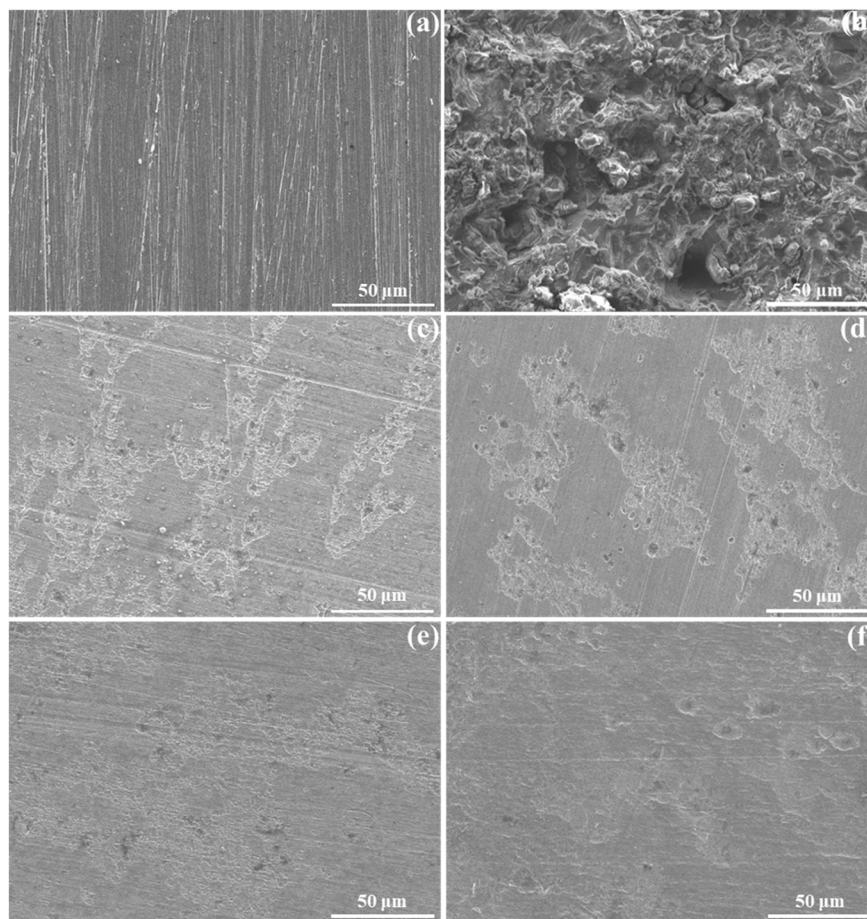
Fig. 5 Surface morphology of steel: (a) after grinding and after 24 h OCP in the acid solution with (b) 0, (c) 500, (d) 1000, (e) 1500, and (f) 2000 ppm BSWE additions.

E_b ~720 eV. This suggests that either another component is generated on the surface of the steel or that the subsequent build up of molecular components from the BSWE is responsible for the adsorption process of the inhibitor on the steel surface. The presence of Fe bonding-based products was visualized through the C 1s and O 1s spectra. The C 1s spectrum in Fig. 6(c) showed the appearance of organic products derived on the steel surface during the corrosion process. Peaks position at 284.8 eV and 284.5 eV corresponded to the chemical states C–C and C=C, respectively.[41] Based on the initial chemical composition of C-containing steels, it was predicted the formation of various corrosion products, with a peak at 288–289 eV corresponding to C=O and O–C=O bonds. These results support the theory that the donor/acceptor mechanism generates through the bond between the C atoms in the organic compounds detected in BSWE and the Fe metal. Notably, when the BSWE inhibitor was added, a strong C 1s peak appeared in all three mentioned peaks, with the highest intensity observed at the 284.5 eV peak, suggesting the formation of products containing C=C bonds. The O 1s spectrum in Fig. 6(d) exhibited different peaks representing the oxidation states of oxygen in the absence of inhibitors. These peaks correspond to various corrosion products, such as metal oxides, metal

carbonates, and organic C–O compounds with binding energies of 529–530 eV, 531.5–532 eV, and 533 eV. In the presence of inhibitors (blue line), the chemical state peaks of O 1s decreased to only two main peaks at E_b ~530.8 eV and 532.7 eV, indicating the presence of organic corrosion products. These chemical states represent organic C=O, C–O, and metal carbonates. This observation demonstrates a clear relationship between the products formed on the steel surface when the inhibitor is added, as seen in the C 1s, O 1s, and Fe 2p spectra. Accordingly, it can be predicted that the presence of BSWE as an inhibitor leads to the formation of corrosion products that act as a protective layer, preventing direct interaction between the steel and the corrosive environment. This ultimately minimises the steel's reactions to the environment. These results are consistent with previous findings (electrochemical and surface analyses) providing further evidence of the enhanced protective performance of mild steel in the presence of BSWE. The results obtained from the analysis of compound concentrations in the BSWE inhibitor using gas chromatography-mass spectrometry (GC-MS), as depicted in Fig. S3 and Table S2.† These findings demonstrate the consistent effects and reliable analytical results, indicating their suitability for identifying organic products. The presence of compounds in BSWE directly impacts
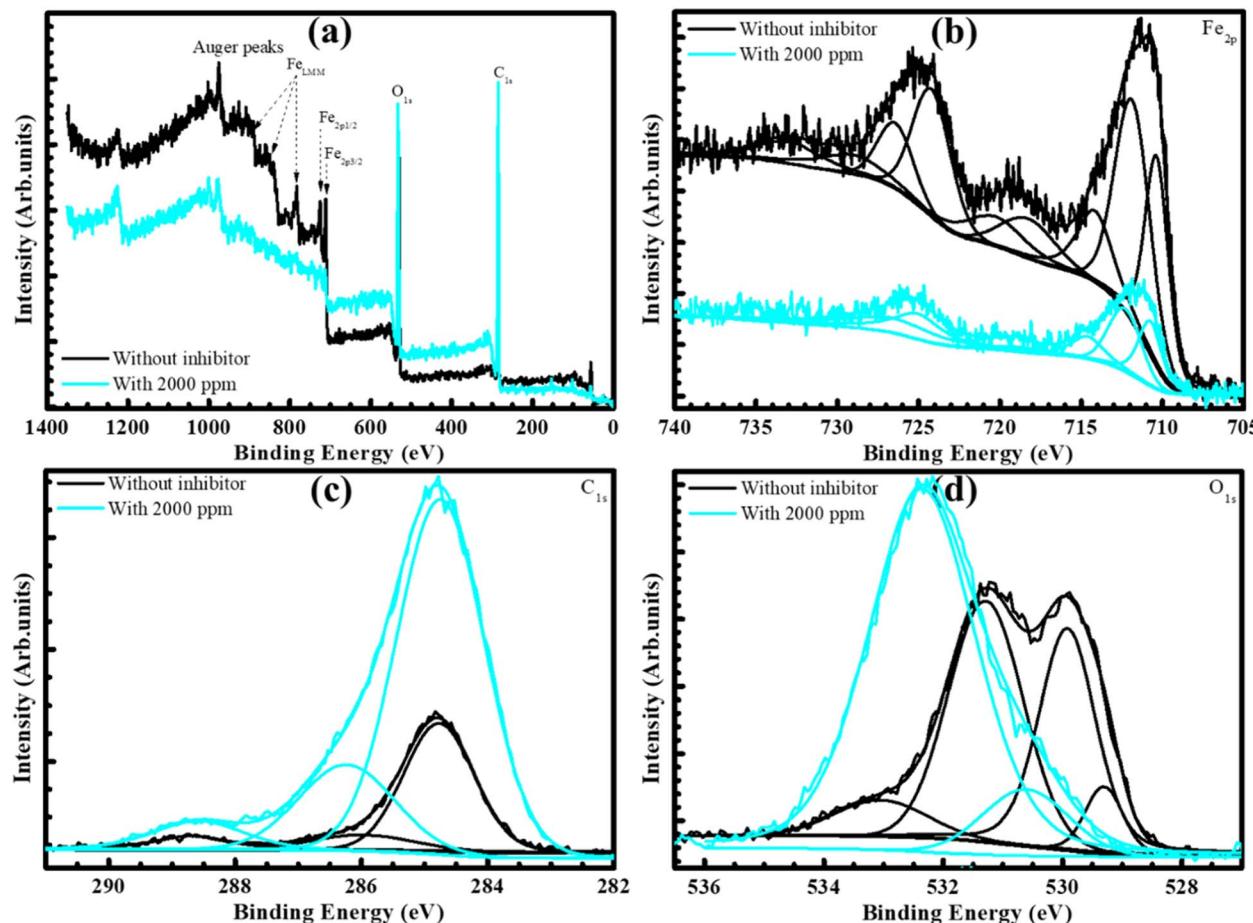
Fig. 6 (a) Wide-scan and narrow-scan XPS spectra of (b) Fe, (c) C and (d) O existence on the steel surfaces after 24 h OCP in the investigated solutions containing 0 and 2000 ppm BSWE.

on the inhibitor activities. Although there is a lack of research on the individual effects of each substance in limiting steel corrosion, our study predicts their potential and lays the foundation for future investigations in this field.

DFT quantum chemical parameters for MC1 are presented in Fig. 7(a), the MC1's structure consists of two separate parts connected by an amide functional group, one is just a hydrocarbon branch, and the other is a branch containing functional groups. It is expected that the most active regions of MC1 would be in part containing functional groups. Due to the electron-withdrawal effect of the aromatic ring and two oxygen atoms (of hydroxyl and ether groups) at one end, an electron-rich region was established at these groups' sites. This effect led to the formation of the HOMO and f(−) areas on π-bonds and these oxygen atoms.[42] As a result, the electron-deficient carbons of the aromatic ring became more positive and facilitated the formation of the LUMO and f(+) areas on these sites. In MC1, the HOMO/f(−) and LUMO/f(+) areas developed in the same direction but settled in different locations. This configuration helps form a dipole on one arm of MC1 and improves the adsorption of MC1 on surfaces. DFT quantum chemical parameters for MC2 are presented in Fig. 7(b), MC2's molecular structure is quite similar to MC1, differing only in a C=C

double bond of the hydrocarbon branch. Fig. 7(b) demonstrates that the electron-withdrawing effect in MC2 is identical to that of MC1, reflected in the formation of HOMO and f(−) regions at π-bonds of the aromatic ring and two oxygen atoms of functional groups. Besides, LUMO and f(+) areas are established at carbon atoms of the aromatic ring due to electron shortage at these sites. To compare Fig. 7(a and b), it was found that the presence (at MC1) and absence (at MC2) of the C=C double bond on the hydrocarbon arm did not significantly affect the MO's distribution in each substance. The main difference between MC1 and MC2 comes from the spatial configuration of these two substances, which in turn leads to an (albeit small) difference between their MO's distributions. The active regions of MC2 (HOMO/LUMO, f(−)/f(+), similar to MC1) will be the binding sites when the substance is adsorbed on a surface (i.e., a steel surface).

DFT quantum chemical parameters for MC3 are presented in Fig. 7(c), distinct from MC1 and MC2, MC3 is a simple molecule with two spiro-connected orthogonal cycloalkane rings and a C=O double bond of the ketone functional group. The active ketone group is expected to determine the formation of electronic regions in MC3, including HOMO/LUMO and f(−)/f(+). Fig. 7(c) shows that, while HOMO and f(−) regions of MC3 are
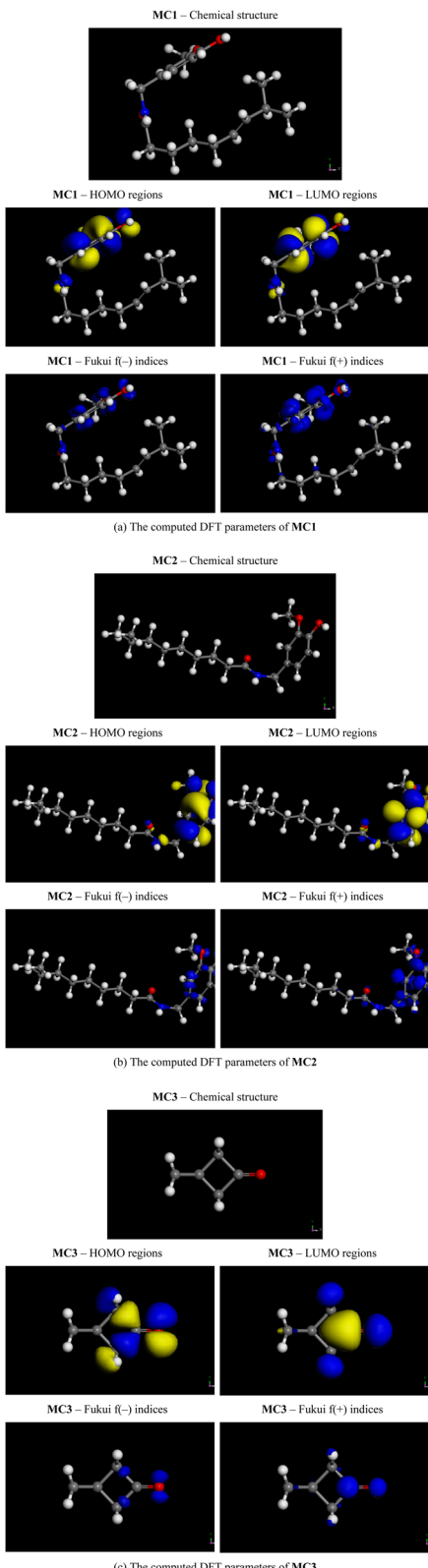
Fig. 7 Computed quantum chemical properties of three MC substances (MC1 – (a), MC2 – (b), and MC3 – (c)), comprising the frontier molecular orbitals (HOMO and LUMO), the Fukui electro/nucleophilic indices (f(−) and f(+)). The calculation was conducted by the DMol³ module of MS, which applied the B3LYP-D/DNP//B3LYP-D/DNP level of theory. The colored atoms are white – hydrogen, grey – carbon, red – oxygen, and blue – nitrogen.

formed around the ketone functional group in one direction (xOy), LUMO and f(+) parts grow in the perpendicular (orthogonal) direction (Oz). Specifically, HOMO regions are concentrated around the oxygen atom in MC3 because this atom attracts electrons of the whole structure towards it. Besides, two carbon atoms of the 4-carbon ring are simultaneously suffered two effects, including the electron-withdrawing effect of the C=O functional group (right side) and the electron repulsion effect of the 3-carbon ring (left side). Combining these two effects establishes high electron density regions at these atoms, leading to the formation of the other parts of the HOMO region in MC3. In contrast, the electron-deficient carbon atom of the ketone group became more positive and formed a LUMO region at its site. In MC3, the HOMO/f(−) regions and LUMO/f(+) are located in different locations except for parts on the oxygen atom. Besides, the orthogonal orientation of the two cycloalkane rings and the inflexibility of the ketone group all lead to limited adsorption of MC3 on the adsorbent, such as steel surface. It can be concluded that the protection effectiveness of MC3 is relatively low compared to MC1 and MC2. The MD final snapshots (at 1.0 ns trajectory, with the settings as described in the experimental section) for all MC substances at two investigated temperatures (298 and 333 K) are presented in Fig. 8. The simulation box dimensions are varied to ensure that the matter density in the boxes is always approximately 1.0 g cm⁻³ during the MD simulation. As seen in Fig. 8, all MC molecules have adhered to the steel substrate after simulations (at different temperatures), which points out three substances are heat stable and can establish protective coatings on the substrate. While MC1 and MC2 molecules bent their structures to attach the whole system to the steel substrate, the MC3 molecule only bent partially of its structure to the steel substrate. Thus, while the binding sites of MC1 and MC2 remained unchanged, two cycloalkane rings of MC3 alternately adhered to the steel surface during the MD simulation. This phenomenon indicates that the adsorption of MC3 onto the steel substrate is less stable than MC1 and MC2.

It can be concluded that all MC substances are potential steel corrosion inhibitors, and the inhibition performance of MC1 and MC2 are comparable but better than that of MC3. A quantitative analysis of the adhesion energies of MC1, MC2, and MC3 on the steel substrate was evaluated based on E_b and E_b per atom results, as present in Table 2. Following Table 2, MC2 has the highest E_b and E_b per atom at 298 K (5.21 and 0.10 eV, respectively), MC1 has the highest E_b and E_b per atom at 333 K (4.90 and 0.10 eV), and MC3 has the lowest E_b and E_b per atom at the two temperatures. Note that E_b and E_b per atom values of MC3 are tiny compared to the other two substances (from 8.6 to 10.4 times smaller), as expected from Fig. 8 analysis. Therefore, MC1 and MC2 are possible as anti-corrosion additives for steel in the investigated environment, while MC3 is not. Considering the heat-stability of MC1 and MC2, Table 2 reveals that both E_b and E_b per atom of MC2 increase with increasing temperature from 298 to 333 K. Conversely, E_b and E_b per atom of MC1 decrease with increasing temperature from 298 to 333 K. This increase (and decrease) of E_b and E_b per atom indicates that MC1 is a heat-stable substance and MC2 is a less
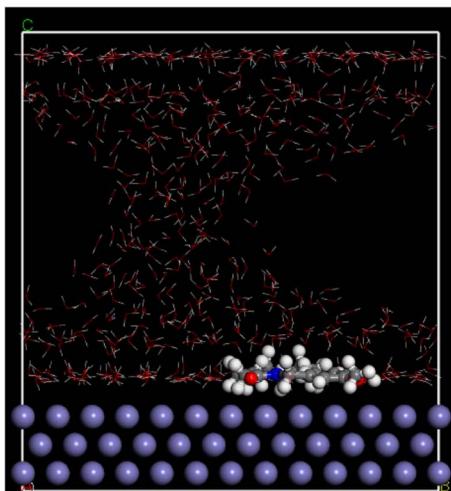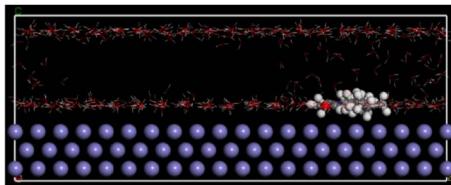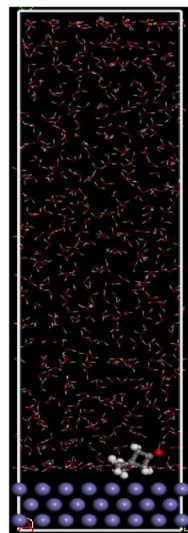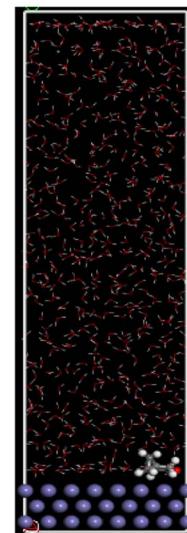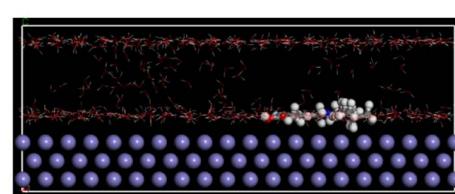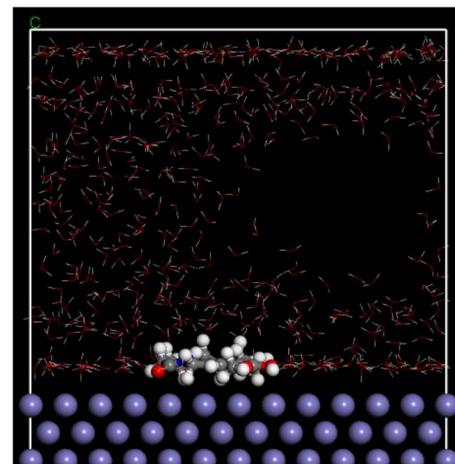
Fig. 8 The MD final snapshot for three MC substances at 298 and 333 K (25 and 40 °C). MD simulation was performed by Forcite module of MS, employed canonical ensemble with Andersen thermostat and COMPASS forcefield, and running for 10^6 steps with a 1.0 fs timestep. The simulation boxes mimicked a steel substrate and an inhibitor molecule (MC1, MC2, or MC3) in a 0.1 M HCl environment. The colored atoms include light blue – iron, white – hydrogen, grey – carbon, red – oxygen, and dark blue – nitrogen.

heat-stable substance. The 11% increase in MC1 and 20% decrease in MC2 (of E_b per atom) are significant, pointing out that the inhibition performance of MC1 is the greatest among the three MC substances. The inhibition performance of three substances could be arranged as follows: MC1 ≈ MC2 ≫ MC3 at 298 K (25 °C), and MC1 > MC2 ≫ MC3 at 333 K (40 °C). Although the E_b and E_b per atom values of MC3 are low compared to MC1 and MC2, it still qualifies as an effective inhibitor under the investigated conditions. It could be said

that BSWE is likely to be an effective corrosion inhibitor in low concentration HCl media. The MD simulation results suggest the inhibitor selection for steel, that is, MC1 or MC2 (or both) at low temperatures (such as room temperature) and MC1 at higher temperatures.

Based on the analysis findings, it was observed that BSWE acted as a mixed type of corrosion inhibitor for mild steel. The electrochemical behaviors showed that the potential polarization curves of samples immersed in a corrosive solution with

Table 2 Binding energies (E_b) and binding energy per atom (E_b per atom) for MC substances are computed at the final stages (after 1.0 ns/1.0 fs trajectory at 298 and 333 K, employed canonical ensemble with COMPASS forcefield and Andersen thermostat)

	MC1		MC2		MC3	
	E_b (eV)	E_b per atom (eV)	E_b (eV)	E_b per atom (eV)	E_b (eV)	E_b per atom (eV)
298 K	4.55	0.09	5.21	0.10	0.50	0.03
333 K	4.90	0.10	4.13	0.08	0.57	0.04

different BSWE concentrations reflected the steel surface in the early stages of corrosion. The initial corrosion primarily focused on impurities or lattice dislocations on the steel surface as shown in Fig. S4.† The presence of chloride ions in the corrosive solution was identified as a significant factor in surface corrosion. The corrosion process intensified over time, resulting in the formation of pits on the mild steel surface and the creation of corrosion products that either separated and fell into the solution or adhered to the steel surface. Additionally, as shown in Fig. 5(a), certain locations experienced more severe corrosion or became areas where more corrosion products formed. The addition of BSWE displayed a tendency to mitigate both anode and cathode reactions, serving as a typed corrosion inhibitor. When considering the corrosion mechanism, two scenarios can be considered, including corrosion without inhibitors and corrosion with inhibitors at varying concentrations. In the absence of the BSWE inhibitor, the steel surface is susceptible to Cl^- ion attack, leading to the generation of corrosion products and dissolution of steel into Fe^{n+} ions, as identified through XPS techniques. Conversely, when the steel was immersed in an HCl solution with the corrosion inhibitor BSWE, its components (COO^-, $C{=}O$, and OH^- groups) bonded with both Fe^{n+} ions and other metal ions in the composition of mild steel. This bonding resulted in the formation of complexes, observed in the SEM images (Fig. 5). Consequently, a protective film formed on the steel surface can prevent direct interaction with the corrosive solution and enhance the corrosion resistance of the mild steel. BSWE demonstrated its ability to bond with the steel surface, creating a stable, continuous, and protective film that provides the inhibitor concentration was appropriate. At the investigated concentrations, the initial addition of the inhibitor was relatively low, leading to the formation of a self-protective film, albeit unevenly, and it does not entirely cover the entire surface, allowing localized corrosion processes. In the corrosive solution with varying inhibitor concentrations, the density and coverage of the protective coating increased on the steel surface. The protective film completely covered the steel surface at a concentration of 1500 ppm BSWE, resulting in inhibiting the corrosion reaction and obstructing the active locations on the steel surface. The presence of functional groups in organic structures present in BSWE indicates that the chemical mechanism is responsible for creating a protective film on the steel surface. In summary, BSWE considerably reduced the corrosion rate of mild steel.

This can be achieved through film formation, which impedes the inward diffusion of corrosive species into the underlying substrate. Furthermore, the DFT quantum chemical parameters for the three different MC substances were studied, and it was found that their molecular structures influenced on their corrosion inhibition performance. MC1 and MC2 exhibited similar molecular structures except for the presence of a $C{=}C$ double bond in the hydrocarbon branch of MC1. However, this difference did not have a significant effect on the distribution of MOs in the substances. The active regions of MC1 and MC2 were the binding sites for the substances when they adsorbed on the steel surface. MC3, on the other hand, had a different molecular structure with two spiro-connected orthogonal cycloalkane rings and a $C{=}O$ double bond of the ketone group. The orientation of the two cycloalkane rings and the inflexibility of the ketone group limited the adsorption of MC3 on the adsorbent, resulting in a relatively low protective effectiveness compared to MC1 and MC2. Finally, MD simulations showed that all MC substances adhered to the steel substrate, but the adsorption of MC3 on the steel substrate was less stable than MC1 and MC2. In conclusion, all MC substances are potential corrosion inhibitors for steel, and MC1 and MC2 have comparable inhibition performances.

The presence of organic compounds with varying concentrations of BSWE is believed to contribute to slowing down the corrosion process. This inhibition mechanism is catalyzed by three main organic compounds including capsaicin, dihydrocapsaicin, and spirohexan-5-one. On one end, the electron-withdrawing effect of the aromatic ring and the two oxygen atoms (from the hydroxyl and ether groups) establish an electron-rich region while the electron-deficient carbon atoms of the aromatic ring become more active, creating an active region. Additionally, according to Valence Bond Theory, iron (Fe) possesses empty d-orbitals that readily accept electrons from the inhibitor provided by heterojunctions. These organic compound inhibitors adsorb onto the metal surface, forming covalent bonds. By covering the entire metal surface area with a film layer thicker than a monolayer, the structure of the electrical double layer at the metal surface is altered. As a result, the steel surface is protected from encountering corrosive ions, such as H^+ and Cl^-, effectively preventing metal dissolution and reducing corrosion rates, as shown in Fig. 9. These studies indicate that BSWE creates a protective layer on the mild steel surface, which can help steel from corrosion in an aggressive electrolyte. Therefore, banana sap extract can be considered a good inhibitor for mild steel operating in an acidic medium. Table S3† presents an overview of the ability of various tree resin (sap/gum) extracts to inhibit corrosion, including the type of corrosion medium, the ideal concentration of inhibitor, and the associated inhibitory effect.[43–51] The results of the table demonstrate the feasibility of using tree resin as an effective corrosion inhibitor, a practice that has been employed for a long time, although some types have not yet achieved the desired level of performance. In light of this, research conducted on banana sap extract has shown that it is a viable substitute. Additionally, the extraction method used is regarded as environmentally benign because water is used as the solvent.
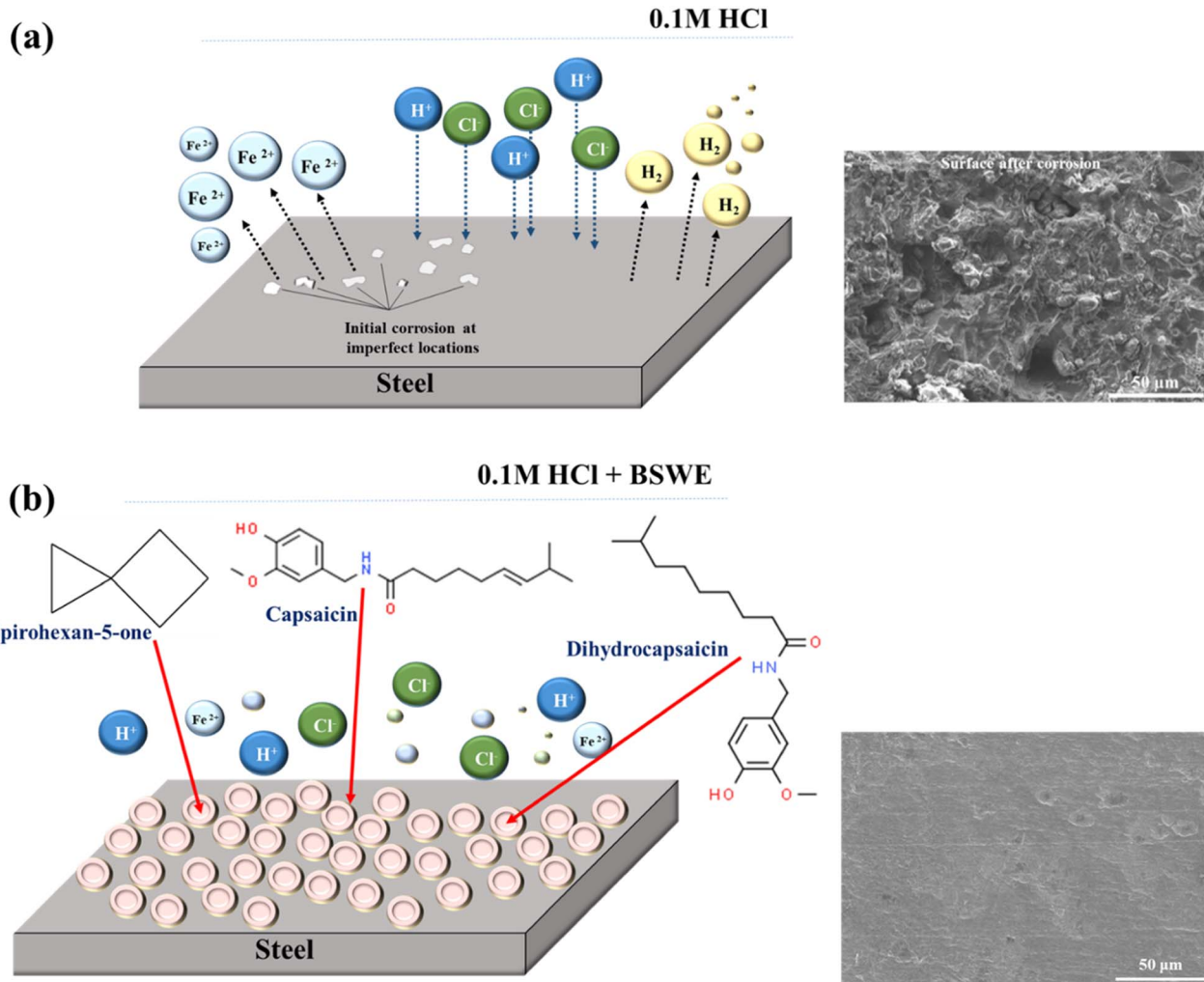
Fig. 9 Mechanisms of mild steel corrosion and inhibition in acidic environments with (a) 0 and (b) 2000 ppm BSWE additions.

On the other hand, the earlier mention of the prevalence of banana plants presents a significant advantage for subsequent research in the future.

4. Conclusions

In this study, banana sap-water extract has been recommended and successfully characterized as a corrosion inhibitor with great effectiveness. LPR measurement showed that polarization resistance increased as a function of time and BSWE concentration, which is consistent with EIS results. Furthermore, potentiodynamic results indicated that BSWE acted as a mixed type of corrosion inhibitor for AS1020 steel in the investigated solution and reached highest efficiency of 94.32% at 2000 ppm. Based on SEM results, a significant amount of etching appeared on the uninhibited substrate surface, and an unambiguous film coverage developed on the substrate of steel bared to the inhibitor corrosion. Accordingly, XPS analysis revealed that the protective film components mainly included the organic groups, present in BSWE incorporated with iron oxide/ hydroxide products, thereby promoting corrosion protection of the steel surface. Alternatively, the identification of substances *via* GC-MS, coupled with DFT and MD simulation calculations, demonstrating the effective adsorption capacity of molecules present in BSWE. The significant inhibition performance suggests that BSWE is a promising inhibitor for promoting corrosion protection of steel in acidic environments. Further work is underway to refine the chemical compounds from the Banana sap extract for use as a corrosion inhibitor and to characterize the stability of this inhibitor system in the aqueous electrolytes.

Author contributions

N. P. V., N. C. T. H.: methodology, investigation, data curation, writing – original draft preparation. T. D. M., L. T. D., N. S. H. V., S. V. P. V., C. P., T. T. P.: methodology, data curation, formal analysis, writing – review & editing. N. N. D.: supervision, resources, conceptualization, investigation, writing – original draft, review & editing, funding acquisition. The final manuscript was read and approved by all writers.

Conflicts of interest

The authors declare that they have no known competing financial interests or personal relationships that could have appeared to influence the work reported in this paper.

Acknowledgements

References

1 U. M. Angst and B. Elsener, *Sci. Adv.*, 2017, **3**, e1700751.

2 G. Koch, J. Varney, N. Thompson, O. Moghissi, M. Gould and J. Payer, *International measures of prevention, application, and economics of corrosion technologies study*. NACE International, Houston, 2016.

3 M. H. Hussin and M. J. Kassim, *Mater. Chem. Phys.*, 2011, **125**, 461–468.

4 H. M. Yang, *Molecules*, 2021, **26**, 3473.

5 J. C. da Rocha, J. A. da Cunha Ponciano Gomes and E. D'Elia, *Corros. Sci.*, 2010, **52**, 2341–2348.

6 M. Ouakki, M. Galai, M. Rbaa, A. S. Abousalem, B. Lakhrissi, M. Ebn Touhami and M. Cherkaoui, *J. Mol. Liq.*, 2020, **319**, 114063.

7 F. EL Hajjaji, R. Salim, E. Ech-chihbi, A. Titi, M. Messali, S. Kaya, B. El Ibrahimi and M. Taleb, *J. Taiwan Inst. Chem. Eng.*, 2021, **123**, 346–362.

8 C. Verma, M. A. Quraishi, A. Alfantazi and K. Y. Rhee, *Adv. Ind. Eng. Polym. Res.*, 2023, **6**, 407–435.

9 S. Karimi, M. Rezaeivala, M. Mokhtare, G. Tuzun and K. Sayin, *J. Taiwan Inst. Chem. Eng.*, 2023, **147**, 104937.

10 M. Goyal, S. Kumar, L. Guo, S. Hamed Alrefaee and C. Verma, *J. Taiwan Inst. Chem. Eng.*, 2021, **123**, 21–33.

11 P. B. Raja and M. G. Sethuraman, *Mater. Lett.*, 2008, **62**, 113–116.

12 L. X. Bach, T. B. N. Dao, K. L. D. Ngo, T. N. Tran, T. L. Minh, H. N. Trong, N. T. Hoai and N. N. Dang, *J. Taibah Univ. Sci.*, 2023, **17**, 2247633.

13 N. R. J. Hynes, R. M. Selvaraj, T. Mohamed, A. M. Mukesh, K. Olfa and M. P. Nikolova, *Chem. Pap.*, 2021, **75**, 1165–1174.

14 M. Manssouri, M. Znini, Z. Lakbaibi, A. Ansari and Y. El Ouadi, *Chem. Pap.*, 2021, **75**, 1103–1114.

15 M. A. Arenas, A. Conde and J. J. De Damborenea, *Corros. Sci.*, 2002, **44**, 511–520.

16 S. Paul and I. Koley, *J. Bio- Tribo-Corros.*, 2016, **2**, 1–9.

17 B. X. Vuong, T. L. Huynh, T. Q. N. Tran, S. V. P. Vattikuti, T. D. Manh, P. Nguyen-Tri, A. T. Nguyen, P. V. Hien and N. N. Dang, *Mater. Today Commun.*, 2022, **31**, 103641.

18 H. Wei, B. Heidarshenas, L. Zhou, G. Hussain, Q. Li and K. K. Ostrikov, *Mater. Today Sustain.*, 2020, **10**, 100044.

19 F. Kaya, R. Solmaz and İ. H. Geçibesler, *J. Taiwan Inst. Chem. Eng.*, 2023, **143**, 104712.

20 H. A. Fetouh, A. Hefnawy, A. M. Attia and E. Ali, *J. Mol. Liq.*, 2020, **319**, 114355.

21 C. Monticelli, *Encyclopedia of Interfacial Chemistry: Surface Science and Electrochemistry*, 2018, pp. 164–171.

22 A. Zakeri, E. Bahmani and A. S. R. Aghdam, *Corros. Commun.*, 2022, **5**, 25–38.

23 N. Hossain, M. A. Chowdhury, M. Rana, M. Hassan and S. Islam, *Results Eng.*, 2022, **14**, 100438.

24 H. Baeza, M. Guzman, P. Ortega and L. Vare, *J. Chil. Chem. Soc.*, 2003, **48**, 23–28.

25 N. Keivani Rad, M. Mohri, H. A. Seifi and A. Haghparast, *Vet. Med. Sci.*, 2021, **7**, 876–887.

26 M. F. Afzal, W. Khalid, A. Akram, M. A. Khalid, M. Zubair, S. Kauser, K. A. Mohamedahmed, A. Aziz and S. A. Siddiqui, *Int. J. Food Prop.*, 2022, **25**, 2286–2300.

27 L. Guo, C. Verma and D. Zhang, *Eco-Friendly Corrosion Inhibitors: Principles, Designing and Applications*, Elsevier, 2022.

28 K. Soorianathasundaram, C. K. Narayana and G. Paliyath, *Encyclopedia of Food and Health*, 2016, pp. 320–327.

29 D. Mohapatra, S. Mishra and N. Sutar, *J. Sci. Ind. Res.*, 2010, **69**, 323–329.

30 V. Paul, K. Kanny and G. G. Redhi, *Ind. Crops Prod.*, 2013, **43**, 496–505.

31 P. I. Murungi, A. A. Sulaimon, O. Ssembatya and P. Nwankwo, *Society of Petroleum Engineers - SPE Nigeria Annual International Conference and Exhibition*, Nigeria, 2022.

32 G. Gupta, S. Saxena, M. Baranwal and M. S. Reddy, *Biologia*, 2022, **77**, 2989–3000.

33 H. Pasdar, N. E. Fard and M. Rezvani, *Appl. Phys. A: Mater. Sci. Process.*, 2023, **129**, 380.

34 A. Rahmanzadeh, M. Rezvani, M. D. Ganji and M. T. Moghim, *Mater. Today Commun.*, 2023, **36**, 106946.

35 J. R. MacDonald, *Impedance Spectroscopy*, Wiley, New York, 1987.

36 N. D. Nam, M. Mathesh, B. Hinton, M. J. Y. Tan and M. Forsyth, *J. Electrochem. Soc.*, 2014, **161**, C527–C534.

37 J. F. Moulder, W. F. Stickle, P. E. Sobol and K. D. Bomben, *Handbook of X-Ray Photoelectron Spectroscopy*, Perkin-Elmer Corporation, Minnesota, USA, 1992.

38 G. Pető, I. Dézsi, L. F. Kiss, Z. E. Horváth, D. Oszetzky, A. Nagy, G. Molnár, Cs. S. Daróczi, K. Frey and A. Horváth, *Vacuum*, 2020, **175**, 109270.

39 D. L. Peng, K. Sumiyama, M. Oku, T. J. Konno, K. Wagatsuma and K. Suzuki, *J. Mater. Sci.*, 1999, **34**, 4623–4628.

40 A. P. Grosvenor, B. A. Kobe, M. C. Biesinger and N. S. McIntyre, *Surf. Interface Anal.*, 2004, **36**, 1564–1574.

41 D. Fang, F. He, J. Xie and L. Xue, *J. Wuhan Univ. Technol., Mater. Sci. Ed.*, 2020, **35**, 711–718.

42 M. Mohammadzaheri, S. Jamehbozorgi, M. D. Ganji, M. Rezvani and Z. Javanshir, *Phys. Chem. Chem. Phys.*, 2023, **25**, 21492–21508.

43 N. B. Iroha and A. O. James, *J. Chem. Soc. Niger.*, 2018, **43**, 510–517.

44 M. Behpour, S. M. Ghoreishi, M. Khayatkashani and N. Soltan, *Corros. Sci.*, 2011, **53**, 2489–2501.

45 S. A. Umoren and U. F. Ekanem, *Chem. Eng. Commun.*, 2010, **197**, 1339–1356.

46 M. Manickam, D. Sivakumar, B. Thirumalairaj and M. Jaganathan, *Adv. Chem. Phys.*, 2016, **2016**, 1–12.

47 M. Mobin, M. Basik and J. Aslam, *J. Mol. Liq.*, 2018, **263**, 174–186.

48 P. O. Ameh, *J. Taibah Univ. Sci.*, 2018, **12**, 783–795.

49 M. Abdallah, *Port. Electrochim. Acta*, 2004, **22**, 161–175.

50 L. Guo, R. Zhang, B. Tan, W. Li, H. Liu and S. Wu, *J. Mol. Liq.*, 2020, **310**, 113239.

51 I. C. Ekeke, S. O. Umosah and A. C. Nkwocha, *International Journal of Innovative Science and Research Technology*, 2021, **6**, 659–664.